

Time-frequency methods for detecting spike activity of stomach

A. Akin H. H. Sun

School of Biomedical Engineering, Science and Health Systems, Drexel University, Philadelphia, PA 19104, USA

Abstract—It has been hypothesised by many researchers that the spike activity signals of the stomach are responsible for triggering peristaltic contractions. Since most gastric motility disorders include an abnormality in the contraction pattern, it is very important to access this information non-invasively. The aim in this study is to use abdominal electrogastrogram (EGG) signals to detect the spike activity signals generated by the serosa of the stomach, and hence provide clinicians with a better method to monitor the motility state of the stomach. Through second and third-order spectral estimations performed on the serosal data obtained from canine experiments, it was concluded that the spike activity in serosal signals occupies a frequency range of 50–80 cycles per minute. An increase in this frequency range during strong antral contractions was observed both in the serosal and cutaneous power spectra. By using the 'continuous wavelet transform' with respect to a modified Morlet wavelet, the spike activity signals generated from the serosa of the stomach can be detected and quantified in time from the cutaneous EGG records. During phase III contraction episodes, a detection accuracy of up to 96% from the cutaneous EGG recordings was calculated based on the scored serosal spike activities simultaneously recorded.

Keywords—Electrogastrogram, Spike activity, Continuous wavelet transform, Modified Morlet wavelet

Med. Biol. Eng. Comput., 1999, 37, 381–390

1 Introduction

SINCE THE 1950s, scientists have been studying the use of the electrogastrogram (EGG) with advanced electrical equipment that allowed them to record the electrical rhythm of the stomach. They discovered that the stomach was electrically active and that the slow-wave depolarisations of this activity are generated by a neural network called the interstitial cells of Cajal (ICC) that resides between the two muscle layers (the longitudinal and circular muscles) and at submucosal borders of the circular muscle. It is assumed that the electrical rhythm is propagated via electrical couplings between the neurons of this extensive ICC network and is thus carried throughout the GI tract with differing frequencies. It was also observed that contractions are the product of some high frequency action potentials either superimposed on the plateau phases of, or in between, slow-wave depolarisations (LIU *et al.*, 1995; SANDERS, 1996). Slow-wave depolarisations have also been called the 'basic electrical rhythm' (BER), 'electrical control activity' (ECA) or simply the slow-wave. The higher frequency action potential has been named the 'electrical response activity' (ERA), 'spike like action potentials' (SLAP) or just spike activity. When spikes occur, they usually entrain the slow wave and strong contractions are seen (YOU and CHEY, 1984;

ATANASSOVA *et al.*, 1995). A widely held view among the researchers in this field is that the higher the frequency and the longer the duration of the spike activity, the stronger the contractions. Clinical evidence suggests that the cause of most gastrointestinal diseases (i.e. stress-related motility disorders, nausea, vomiting, dyspepsia, impaired gastric emptying, gastroparesis, gastric ulcer, gastric dysrhythmias) are related to some sort of disturbance in the motility of the stomach (AMY, 1975; CHEN and MCCALLUM, 1993). Hence, detection of any motility disorder *non-invasively* has diagnostic value. Currently, invasive techniques such as intraluminal manometry, fluoroscopy or endoscopy are used in determining the rhythm and strength of the contractions. The relationship between the EGG and gastric motility has been widely investigated (SMOUT *et al.*, 1980; YOU and CHEY, 1984; KOCH and STERN, 1994). Based on these ideas, we hypothesised that surface EGG signals can be utilised to access this information non-invasively. However, a new signal processing method has to be developed to detect serosal spike activities in both magnitude and frequency from cutaneous EGG recordings.

There are certain complications in the detection of these small amplitude, high frequency signals from the surface. A detailed engineering approach to this problem that could shed light on the properties of spike activity signals is still lacking. Although models have been proposed for the generation and propagation of slow waves (MIRIZZI and STELLA, 1985; MIRIZZI *et al.*, 1986; MINTCHEV and BOWES, 1997), none of these models address the simulation of spike activity. One problem in locating spike activity when compared with the

Correspondence should be addressed to Professor Hun H. Sun; email: sun@cbis.ecs.drexel.edu

First received 21 August 1998 and in final form 12 January 1999

© IFMBE: 1999

slow wave is that it does not propagate throughout the stomach. The slow wave spreads readily into both longitudinal and circular muscles (CHEN and MCCALLUM, 1991, 1993; LIU *et al.*, 1995). This localised behaviour of the spike activity can be observed experimentally: if a series of electrodes are placed on the serosal wall of the stomach along the Greater Curvature, spike activity can be detected only at a certain part of the stomach, and it stays local to that region (LIU *et al.*, 1995). This could create major problems when trying to record these locally generated signals from the abdominal surface. This localised behaviour of the spike activity makes it difficult to model using a propagating dipole model.

Another major concern is the electrical properties of the layers underlying the skin, including the abdominal muscles, fat, omentum, peritoneum and vessels. These layers may have distorting effects on the original serosal signal resulting in the attenuation, smearing, and smoothing of the information-bearing data (BRADSHAW, 1995). Although this assumption needs to be verified by a volume conductor approach, we can, without loss of generality, conclude that the resultant signal at the surface is generally weak in amplitude and contaminated by many other electrophysiological signals, such as the ECG, the EMG of abdominal muscles or the respiratory signals. Therefore, the exact location of the surface electrodes can have a major influence on the detection of serosal spike activities. On the other hand, it has been observed, through correlation studies, that the slow wave tends to pass readily through the tissues without being heavily attenuated. This is why all previous research has concentrated on the energy changes of the EGG in the frequency range 1 to 18 cycles per minute.

This paper reports investigations of the time–frequency characteristics of the serosal signals when the stomach is at rest (no spike activity), and compares the results with signals recorded when there are contractions (slow waves followed by spike activity). The slow wave and slow wave combined with spike activity are modelled as stationary random processes. Two different power spectrum estimators are used in estimating the frequency response (range) of spike activities. The autoregressive method is based on the second-order moments of a signal whereas the bispectrum-based method utilises the third-order moments in identifying the impulse response of the signal (NIKIAS and PETROPULU, 1993). It is shown that bispectrum-based power spectrum estimation yields a clearer distinction between the spectra of the serosal signal with and without spike activity. We conclude from the analyses of dog experiments that the frequency range of spike activity falls between 50 and 80 cycles per minute.

We then try to determine whether the stomach's localised electrical activity actually penetrates the abdominal layers by studying the correlation between the two sets of recordings: serosal and abdominal (surface) data. The *Power Dynamics* (PD) method is used for correlation study, as has been used by others (SMOUT *et al.*, 1980; KOCH and STERN, 1994; MINTCHEV and STICKEL, 1997a, 1997b) to investigate the reliability of EGG. It has been shown that when the energy progression of the slow wave activity at a certain distinct frequency is tracked (i.e. three cycles per minute), the serosal and abdominal signals portray the same trend. We therefore apply a similar approach to correlate the energy progressions of the two sets of recordings (serosal and surface) but instead *within certain frequency bands*. Tracking the energy changes in certain frequency bands provides an indication of whether some of these electrical activities are reflected on the surface. Since we can select the frequency band for the energy correlation analysis, we termed the method the *Selective Power Dynamics*, SPD. This method is explained in detail in Section 2.

The results from SPD analysis suggest that accurate detection of spike activity is extremely dependent on the electrode location on the surface of the abdomen. One method is to align the surface electrodes with the axis of the stomach in coronal to anal direction and to acquire signals with a DC amplifier (MIRIZZI and STELLA, 1985; MIRIZZI *et al.*, 1986), then apply appropriate filtering to remove the noise and artifacts. Correlation studies on the SPD are performed between the serosal and surface data. If high correlation occurs, we then use the continuous wavelet transform (CWT) to analyse the data for spike detection. Using this method, we are able to localise the spike activity from both the serosal and surface data, where they match in time and frequency.

2 Methods

2.1 Data acquisition

We have conducted a number of canine experiments where we acquired simultaneous data from the serosal wall of the stomach and the abdominal surface. All the experiments were carried out at the Genesee Hospital of the University of Rochester, Rochester, NY. The data acquisition system consisted of a Grass Polygraph* and an analogue to digital converter board.† We used commercially available data acquisition software** to record EGG data into a PC. The data were sampled at 100 Hz. The digitised data were then further decimated to 4 Hz to eliminate artefacts and interference from other electrophysiological sources. During the experiments, the animals were anaesthetised intravenously (i.v.) with 30 mg kg⁻¹ Nembutal. Platinum bipolar serosal electrodes were implanted surgically to the serosal surface of the stomach along the Greater Curvature approximately 2, 4, 6 and 8 cm from the pylorus as shown in Fig. 1a. In most of these experiments, the electrode closest to the pylorus was used in determining the frequency characteristics of the spike activity. Strain gauges were sutured next to the electrodes at 2 and 6 cm from the pylorus. Simultaneously recorded serosal and surface data can be seen in Fig. 4. The signal in Fig. 4a, was acquired from a region close to caudad corpus.

After the abdominal skin was closed with Dermalon sutures, the skin electrodes were placed on the abdominal surface corresponding to the antral area. Two pairs of skin electrodes were placed after skin preparation by shaving and cleaning with soap and alcohol to reduce skin resistance. We have tried several configurations for recording the EGG data to obtain the highest amplitude signal (see Fig. 1b).

The electrodes were placed on the abdominal surface in accordance with the placement suggestion by MIRIZZI and STELLA (1985) and MIRIZZI *et al.* (1986). The recordings were divided into phases where each phase was either a basal recording or a contraction recording. The contractions were induced by intravenous injection of Erythromycin (0.1–1.0 µg kg⁻¹). The surface signals recorded after such an injection are shown in Fig. 4b.

2.2 Signal processing

In this section we briefly explain the signal processing methods used in pursuing our goals, which are listed as follows:

* Sandhill Data Acquisition System, Model 7.

† National Instruments.

** BioView (Sandhill Science Inc) and LabView.

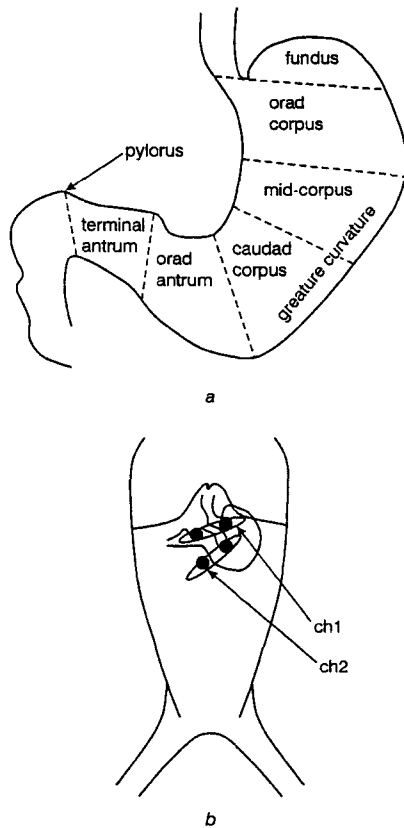


Fig. 1 (a) Placement of electrodes on the canine stomach wall, 2, 4, 6, and 8 cm from the pylorus. (b) Location of the electrodes on the abdominal surface of the dog in supine position. The pairs of electrodes are placed to be aligned with the longitudinal axis of the stomach

- Determine the frequency range of the spike activity.
- Apply the SPD method to determine the correlation between the serosal signal and the abdominal signal.
- Localise the spike activity in both the serosal and abdominal signals using the time–frequency analysis method or the continuous wavelet transform (CWT) developed by Morlet (MORLET and ARENS, 1982).

2.2.1 *Determining the frequency content of spike activity*
 From our experiments and from information deduced from the literature, we conclude that the spike activity is best recorded from the terminal–orad antrum, approximately 2–4 cm from the pylorus (BERNE and LEVY, 1993), as in Fig. 1a. A segment of data with spike activity recorded from Ch 2 (Fig. 1b) can be seen in Fig. 4a.

To determine the frequency range of the spike activity we applied both parametric and non-parametric power spectrum estimators: the auto regressive (AR) method and the bispectrum-based (BiS-based) method. These methods are explained briefly in the following paragraphs. Power spectrum estimators depend on the assumption that the signal is stationary or at least remains stationary in a chosen window. In our case, although the EGG signal is non-stationary in nature, we assume that it remains stationary in a short analysis window. The choice of window size and its effects are discussed in the following sections.

AR method. In this method, it is assumed that the discrete time signal $x(n)$ is the output of a linear time invariant (LTI)

all-pole filter that is excited by a white, zero-mean Gaussian noise $w(n)$ (PROAKIS and MANOLAKIS, 1996). The AR process can be formulated as:

$$x(n) + \sum_{k=1}^p a_k x(n-k) = w(n) \quad (1)$$

Here, we write the z -transform $A(z)$ of the coefficients a_k as $A(z) = \sum_k a_k z^{-k}$, where p is the order of the estimator. The calculation is based on the autocorrelation function of the signal:

$$r_{xx}(m) = \frac{1}{N} \sum_{n=0}^{N-m-1} x^*(n)x(n+m) \quad m \geq 0 \quad (2)$$

where $*$ stands for complex conjugation. Since we are working with real signals, the conjugation operator is omitted. In this equation, the biased estimate of the autocorrelation function is used to ensure that the autocorrelation matrix is positive semidefinite. Calculation of the AR coefficients from the estimate of the autocorrelation function is carried out using the Yule–Walker solution, and the corresponding ‘power spectrum estimate’ (PSE) can then be formulated as:

$$P_{xx}(f) = \frac{\hat{\sigma}_{wp}^2}{\left| 1 + \sum_{k=1}^p \hat{a}_p(k) e^{-j2\pi f k} \right|^2} \quad (3)$$

where $\hat{a}_p(k)$ are estimates of AR coefficients calculated by the Levinson–Durbin algorithm and

$$\hat{\sigma}_{wp}^2 = \tilde{E}_p^f = r_{xx}(0) \prod_{k=1}^p [1 - |\hat{a}_k(k)|^2] \quad (4)$$

is the estimated minimum mean-square value for the p th order predictor (PROAKIS and MANOLAKIS, 1996). In our analysis we use a 10th-order AR process to estimate the power spectrum of the serosal signals. Analysis window duration is 1 minute with 80% overlapping (REDDY *et al.*, 1987). The PSE of the unspiked and spiked activity of serosal signals can be seen in Fig. 2a where clear separation of the PSEs of the two signals cannot be obtained.

Bispectrum-based method. The bispectrum-based method depends on the third-order statistics of the signal whereas the AR method uses the second-order statistics. The assumption is that the probability distribution function of the excitation signal is non-Gaussian. We can express the convolutional model of the measured signal $x(n)$ as:

$$x(n) = \sum_{k=-N}^M h(k)w(n-k) + g(n) \quad (5)$$

where $h(n)$ is the LTI, non-minimum phase system, $w(n)$ this time is the stationary, zero-mean, non-Gaussian, independently identical distributed (i.i.d.) white noise, and $g(n)$ is the additive zero-mean Gaussian white noise, independent of $w(n)$ (NIKIAS and PETROPULU, 1993). The third-order cumulants of the signal $x(n)$ are given by the equation below:

$$r_x(n_1, n_2) = E[x(n)x(n+n_1)x(n+n_2)] \quad (6)$$

where $E[\cdot]$ is the expected value operator. By taking the Fourier transform of this cumulant sequence in eqn. 6, we obtain the bispectrum $B_x(\omega_1, \omega_2)$:

$$B_x(\omega_1, \omega_2) = \sum_{n_1=-\infty}^{\infty} \sum_{n_2=-\infty}^{\infty} r_x(n_1, n_2) e^{-j(\omega_1 n_1 + \omega_2 n_2)} \quad (7)$$

When we substitute eqn. 6 into eqn. 7, we obtain

$$B_x(\omega_1, \omega_2) = \beta H(\omega_1)H(\omega_2)H^*(\omega_1 + \omega_2) + B_g(\omega_1, \omega_2) \quad (8)$$

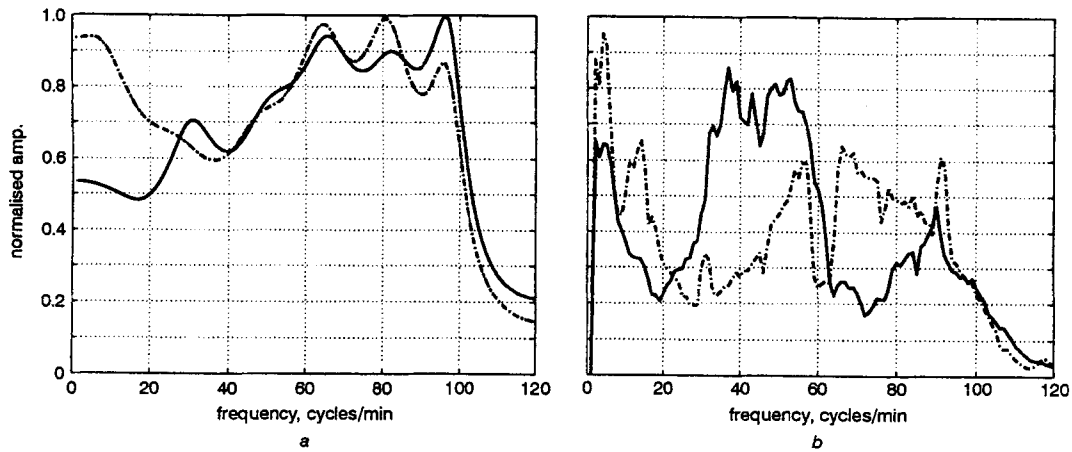


Fig. 2 (a) PSEs from AR method. (b) PSEs from BiS-based method. — no contraction, unspiked data; - - - - contraction, data with spike activity

Here, $\beta = E[w(n)^3]$ and $B_g(\omega_1, \omega_2)$ is the bispectrum of $g(n)$. The advantage of this method is that the bispectrum of the Gaussian noise term becomes null in theory. Hence, the bispectrum operator actually eliminates the effects of any additive Gaussianity to the signal. The goal of this analysis is to reconstruct the impulse response $h(n)$ from the bispectrum $B_x(\omega_1, \omega_2)$ (NIKIAS and PETROPULU, 1993). We then estimate the power spectrum of $h(n)$, $|H(\omega)|^2$, by using the standard periodogram method. In our analysis for estimating the PSE of the spiked versus unspiked activity, among many available methods we adopt the method of ALSHEBEILE and ÇETIN (1990) to obtain $h(n)$. The results of our analysis for $|H(\omega)|^2$ can be seen in Fig. 2b, where a distinct energy increase is observed in the spectrum of the spiked activity with respect to the unspiked activity.

2.2.2 Selective power dynamics (SPD) method In an attempt to perceive whether the energy variations within certain frequency bands of the surface signal follow the serosal signal's energy, we modified the power dynamics method used by Mintchev (MINTCHEV and STICKEL 1997a, b). This method is based on calculating the energies of a signal within certain frequency bands from the periodograms of the signal. First the signal $x(n)$ is multiplied by a window $w(n)$ with length L points and then Fourier transformed (OPPENHEIM and SHAFER, 1989):

$$X(\omega) = \sum_{n=0}^{L-1} x(n)w(n)e^{-j\omega n} \quad (9)$$

To compute the estimate of $X(\omega)$, we use:

$$P_x(\omega) = \frac{1}{LU} |X(\omega)|^2 \quad (10)$$

where U is a constant to normalise the bias in the spectral estimate. Eqn. 10 is called the periodogram if the window used is rectangular (OPPENHEIM and SHAFER, 1989). The total energy, $\varepsilon_x(\omega_1, \omega_2)$, in the interval $[\omega_1, \omega_2]$ is calculated according to the formula below:

$$\varepsilon_x(\omega_1, \omega_2) = \int_{\omega_1}^{\omega_2} P_x(\omega) d\omega \quad (11)$$

The duration of the analysis window $w(n)$ is chosen to be 1 minute and no overlap is allowed. The frequency bands we choose are 1–5, 5–20, 20–50, 50–80 and 80–110 cycles per minute as dictated by the power spectrum analyses (Figs. 2b and 6b). We correlate the selective power dynamics (progres-

sion of ε_x) of the serosal signal to the one calculated for the two surface recordings. Once again our aim is to observe the level of energy penetration to surface data from the serosal signal in various frequency bands. This correlation analysis provides insight into the reliability of EGG data, since it is still disputed whether or not EGG is a sufficiently reliable representation of the gastromyolectric activity to be used as a diagnostic tool, similar to EKG, EEG or EMG (CHEN and MCCALLUM, 1991, 1993; KOCH and STERN, 1994; MINTCHEV and BOWES, 1994; MINTCHEV and STICKEL, 1997a).

2.2.3 Time-frequency representation of spike activity After evaluating the frequency range of the spike activity, we then search for a time-frequency analysis tool that will provide the highest resolution in this frequency range. The continuous wavelets transform (CWT) is a method of representing the frequency contents of a signal in time. It is one of the common time-frequency representations especially applicable to non-stationary data.

In the continuous case, when the real random signal $x(t)$ is considered for a time varying spectral analysis, the first thing we should know *a priori* is whether the signal is stationary or non-stationary. One way of getting around the stationarity problem is to pseudo-stationarise the signal by dividing it into quasistationary segments of equal length. This approach leads to the spectrogram, or the squared magnitude of the 'short time Fourier transform' (STFT) given by the equation:

$$STFT_x(t, \nu) = \left| \int_{-\infty}^{\infty} x(u)w(t-u)e^{-j2\pi\nu u} du \right|^2 \quad (12)$$

Here, a window function $w(t)$ with a finite duration is multiplied by the signal and then slid t points (seconds) in time. To achieve high frequency resolution, the window length should be increased, which results in decreasing the time resolution. If certain properties of the window can be changed continuously so as to compensate for the change in frequency or time resolution, we arrive at the CWT (GROSSMANN *et al.*, 1987; RIOUL and DUHAMEL, 1992):

$$CWT_x(b, a) = \frac{1}{\sqrt{a}} \int x(t)\psi^*\left(\frac{t-b}{a}\right) dt \quad (13)$$

Here $*$ denotes the complex conjugate of the window function $\psi(t)$, and \sqrt{a} is added for energy conservation. Eqn. 13 is defined on the open 'time and scale' half-plane ($b \in \mathbf{R}, a > 0$), hence called the 'time-scale' analysis since the window $\psi(t)$ is scaled by the constant a in time. This procedure, if analysed in

detail, is nothing but a ‘constant-Q filter bank’ approach (VETTERLI and HARLEY, 1992). Eqn. 13 can be written in the Fourier Domain with the help of Parseval’s Identity:

$$CWT_x(b, a) = \frac{\sqrt{a}}{2\pi} \int \hat{\psi}(a\omega) e^{j b \omega} \hat{x}(\omega) d\omega \quad (14)$$

Here $\hat{\cdot}$ denotes Fourier transform. In eqn. 14 we see that the Fourier transform of the signal $x(t)$ is multiplied by the Fourier transform of a scaled version of the window function $\psi(t)$ termed the *mother wavelet*. By scaling the argument of the mother wavelet a times in the frequency domain, we can change its frequency response. Basically, the mother wavelet is an ideal bandpass function that should satisfy the following admissibility conditions (VETTERLI and HARLEY, 1992):

- (a) $2\pi \int \frac{|\hat{\psi}(\omega)|^2}{|\omega|} d\omega < \infty$;
- (b) $\hat{\psi}(0) = 0 \Rightarrow \int \psi(t) dt = 0$;
- (c) $\int t^n \psi(t) dt = 0 \quad n = 0, 1, \dots, N - 1$.

The first condition assures a decay in the Fourier domain which implies that the wavelet has weak convergence and finite energy. It is also necessary to have $\int |x(t)|^2 dt < \infty$ so that the signal is also of finite energy. These two conditions (one for the wavelet and the other for the signal) limit the analysis to the Hilbert space, \mathcal{H} , or the normed linear vector space, $L^2(\mathbf{R})$ (GROSSMANN *et al.*, 1987). The other two conditions ensure that the mother wavelet has zero mean and is differentiable. It is observed that with an arbitrary choice of a ($a \neq 0$), eqn. 13 becomes a highly redundant representation of the signal $x(t)$. As the mother wavelet is scaled so that its oscillating frequency shifts towards higher frequencies, time resolution improves but we lose frequency resolution, as described by the Heisenberg’s Uncertainty Principle (time resolution and frequency resolution cannot be made infinite at the same time) (GROSSMANN *et al.*, 1987; RIOUL and DUHAMEL, 1992; VETTERLI and HARLEY, 1992).

In this study, we use the *Morlet wavelet* as the mother wavelet which is a modulated Gaussian with the time domain equation and Fourier transform pair as follows:

$$\psi(t) = \frac{1}{\sqrt{2\pi}} e^{j\omega_0 t} e^{-(t^2/2)} \iff \hat{\psi}(\omega) = e^{-[(\omega - \omega_0)^2/2]} \quad (15)$$

Here, ω_0 is chosen such that the second maximum of the real part of the wavelet, $\Re\{\psi(t)\}$, $t > 0$, is half the first one at $t = 0$. Usually this value is $\omega_0 = \pi\sqrt{2}/\ln 2 = 5.336$ (GROSSMANN *et al.*, 1987). With this value of ω_0 , the bandpass filter $\psi(\omega)$ is localised at the centre of the frequency plane. In a real case we do not work with continuous signals and filters but rather with discrete signals and filters which have finite length. Therefore for the discrete case, eqn. 13 with respect to the wavelet $\psi(t)$ can be discretised as follows:

$$CWT_x(iT_s, a) = T_s \frac{1}{\sqrt{a}} \sum_n x(nT_s) \psi^* \left(\frac{(n-i)T_s}{a} \right) \quad (16)$$

Here T_s is the sampling interval, and i is the integer sample number (DUTILLEUX, 1987). In our analysis, we use a slightly modified form of the Morlet wavelet given in eqn. 15. Since we make use of the discretised version of eqn. 14, we give only the Fourier domain representation of the wavelet used as:

$$\hat{\psi}(\omega) = e^{-[(\omega_s - \omega_c)^2/2]} - e^{-[\omega_s^2 + \omega_c^2/2]} \quad (17)$$

Here $\omega_c = N/\xi$, where N is the number of sample points (in our case $N = 512$) of the signal, and ξ is the divisor that sets the centre frequency for the mother wavelet. Figs. 3a and 3b show the wave shapes of the modified adaptive Morlet wavelet for $\xi = 60$ and $\xi = 120$. Details of this work and a proof of

validity can be found in AKIN *et al.* (1997). It has also been shown (AKIN *et al.*, 1997) that the modified Morlet wavelet has increased resolution in the higher frequencies compared to the conventional Morlet wavelet. Figs. 3c and 3d show the corresponding magnitude response for the scaled versions of these mother wavelets.

The scaling is performed on ω such that $\omega_s = \omega/a$, ($0 \leq \omega \leq \pi$), where this time $a = a_0 2^{m/M}$, $m = 0, 2, \dots, M - 1$. Traditionally, $a_0 = 2$ is chosen so that scales increase and decrease in a dyadic fashion. But to enhance the frequency resolution with the compromise of increasing redundancy, M voices can be incorporated into the scaling (RIOUL and DUHAMEL, 1992). In our case, $M = 10$ is used. The effect of adding voices is to achieve a finer scaling or fractional dilation of the mother wavelet, thus increasing the number of bandpass filters that will be produced for one scale (STRANG and NGUYEN, 1996). This phenomenon can be observed when Fig. 3c is compared with Fig. 3d where the magnitude response of filters overlap with a greater percentage in the frequency domain. Hence, in contrast with non-overlapping (dyadic) wavelets, when the voices concept is incorporated, a denser time–frequency tiling can be obtained.

3 Results

Our main objective is to localise the spike activity of the stomach from surface EGG recordings. To accomplish this task we first investigated the serosal signals by comparing the results of two power spectrum estimators as described above, and obtained the frequency range of the spike activity. We processed the serosal recordings with and without spike activity. By comparing the PSEs of these signals, we then found the frequency range of spike activity in the serosal signals. Figs. 2a and 2b show the results of such an analysis. After conducting five dog experiments with eight phases during each one, we average the results obtained from each phase. As can be observed the bispectrum-based approach yields a more distinct change between the PSEs of unspiked and spiked data than the AR-based method. Careful inspection of these plots reveals an increase of energy in the frequency range 60–80 cycles per minute (AKIN *et al.*, 1997, 1998).

Next, we try to validate the assumption that the EGG obtained is a reliable measure of the electrical activity of the stomach (KOCH and STERN, 1994; SMOUT *et al.*, 1980). The method we use is the SPD as explained in Section 2. We analyse the data collected from five different dog experiments, and tabulate the correlation coefficients between the SPDs of serosal and surface recordings for each set of data. Here it might be useful to recall the definition of the correlation coefficient (ρ) between data X and data Y :

$$\rho_{XY} = \frac{\text{Cov}[X, Y]}{\sqrt{\text{Var}[X]\text{Var}[Y]}} \quad (18)$$

In eqn. 18, $\text{Cov}[X, Y]$ is the covariance of the data X and Y , $\text{Var}[X]$ is the variance of X . Table 1 presents the cumulative results of all the experimental data. We exclude data that have a correlation coefficient of less than 0.6. The results show that in each of the frequency ranges, the correlation is relatively high. There are many explanations for not obtaining a higher correlation coefficient which we will discuss in the Conclusions section.

Similarly, when signals recorded from the two surface electrodes (seen in Fig. 1b) are correlated, a high correlation coefficient is obtained. In Table 2 the results of such an analysis are presented.

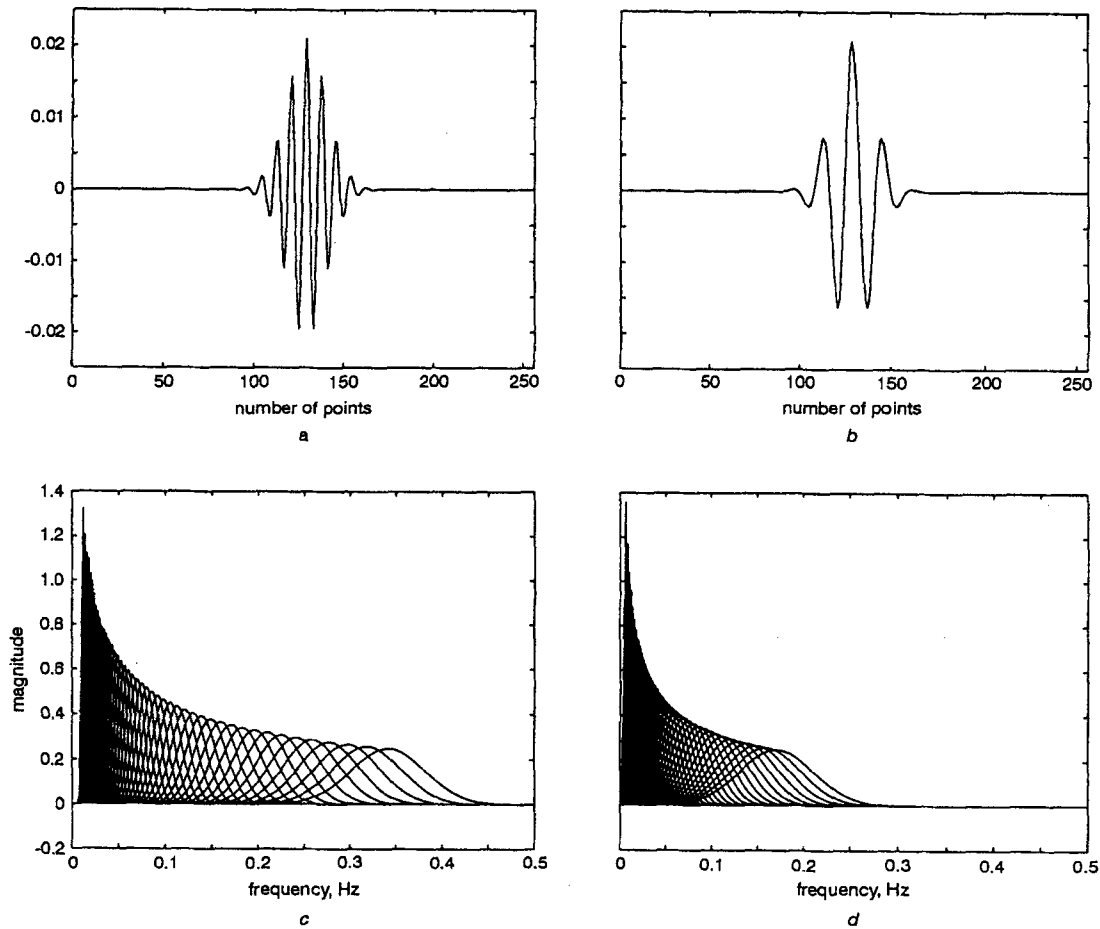


Fig. 3 Morlet wavelets with (a) $\xi = 60$ and (b) $\xi = 120$. (c) and (d) Magnitude response of the scaled versions of the mother wavelets in (a) and (b)

Table 1 Correlation analysis between serosal and surface recordings

Frequency range cycles per minute	Average	SD
1–5	0.79	0.11
5–20	0.79	0.12
20–50	0.78	0.12
50–80	0.80	0.11
80–110	0.78	0.11

Table 2 Correlation analysis between two surface recordings

Frequency range cycles per minute	Average	SD
1–5	0.91	0.07
5–20	0.90	0.09
20–50	0.85	0.12
50–80	0.84	0.12
80–110	0.80	0.12

As the energy in the serosal signal increases, so does the energy in the surface recording. One major problem with correlation analysis is the introduction of a delay factor between the two signals. The autocorrelation coefficient ρ_{XX} of a signal decreases if the lag between the two is increased. However, we know from the volume conductor theory that a biosignal generated internally must be distributed simultaneously on the surface (BRADSHAW, 1995). Hence, when we compute the energy of the pylorus signal and compare it with

the surface signal, we see a delay in the energy increase of the corresponding spike activity. Thus, low correlation will be obtained between the pylorus signal and the surface signal. This low correlation can be increased by lengthening the analysis window to two minutes or by shifting the serosal (surface) signal so that they match each other. In the case of a duration of two or more minutes for the analysis window, the correlation coefficient rises to values of 0.92 and above. The disadvantage of increasing the window length is losing the time resolution. The spike activity is a short duration signal, therefore the window length should be short enough to capture the fast changes in the frequency content of the signal but also long enough to compensate for the slow wave frequency.

In Section 2, we described the two approaches used to determine the frequency range of the spike activity as recorded from the serosa of the stomach. The analysis window chosen for both methods is one minute. The reason for not choosing a shorter window is because, as the window is shortened, the frequency resolution worsens. Also, regular slow waves recorded from the serosa usually resemble bursts (Fig. 4a). When we decrease the length of the window, we see that the spectrum of the burst signal dominates the spike activity's frequency band. So, there is a trade-off between a correlation coefficient that is proportional to the length of the analysis window and the precise frequency content of the spike activity. We chose a window duration of one minute. Our results are confirmed by analysing data obtained from Dr J. D. Chen of the Lynn Institute for Healthcare Research, Oklahoma City, OK. Both methods (AR-based and BiS-based) detected an increase in the energy during contraction (C) episodes at frequencies in the range 50–80 cycles per minute (see Figs. 6a and 6b).

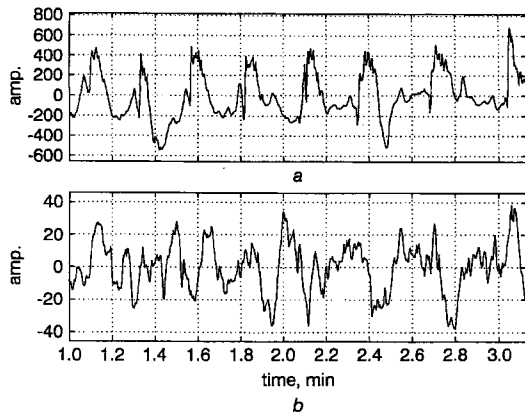


Fig. 4 (a) Serosal recording from terminal antrum. (b) Simultaneous EGG recording from the abdomen. The spike activity can be seen on the plateau phases of the serosal signal (a)

Nevertheless, it should be noted that our results were obtained from signals acquired from dogs under anaesthesia, whereas Dr Chen's recordings were from conscious dogs and the contractions are the result of feeding where the acquisitions were initiated during the postprandial stages. Therefore, slight differences in the frequency ranges of the spike activity are quite natural. We do not have a full explanation of the effects of the anaesthesia but this analysis indicates that there are differences in the signals obtained (compare Figs. 4 and 5).

We used data from a position closest to the pylorus in evaluating the frequency content of the spike activity (see Fig. 1a). The results from the analyses conducted on the new set of data confirmed the same frequency interval for the serosal spike activity as obtained from the Rochester experiments.

We apply the CWT method to detect the serosal spike activity from cutaneous EGG recordings. There are various fast CWT algorithms, and we chose one that depends on the FFT algorithm (RIOUL and DUHAMEL, 1992; VETTERLI and HARLEY, 1992). CWT of the data is calculated for 512 points, which corresponds to 2.13 minutes when the sampling rate is 4 Hz, and 1.76 minutes when it is 5 Hz. The value of ξ as explained in Section 2 is usually chosen between 25 and 29. In Fig. 7, we show the CWT of such an analysis, where a slight shift in the frequency locus of the spike activity between the serosal signal and the surface signal can be seen. However, the main peak occurs at around 60 cycles per minute. Also, most of

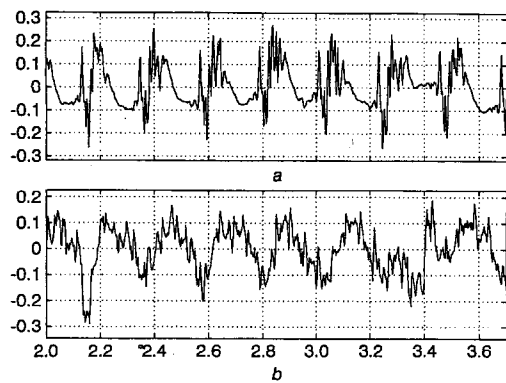


Fig. 5 Serosal data (a), and surface EGG data (b)

the signals between 70 and 80 cycles per minute seem to be stopped by the tissue layers whereas 50–70 cycles per minute signals can be seen at the surface. This could be the reason for the difficulty in obtaining an exact match between the frequencies of the serosal and surface signals. Additional results were performed and they all lead to the same conclusion. The detection accuracy is calculated by a blind study, where the number of contractions indicated by the strain gauge attached to the serosa is compared with the number of spike activities detected from the cutaneous signals. The average detection is found to be 87% for the Rochester experiments, and 96% for the Oklahoma experiments. The reason for the increase in detection ratio is the enhanced strength of the serosal spike activity signals of the Oklahoma experiments. Detailed analyses and results can be found in AKIN (1998).

4 Conclusions

Gastrointestinal motility has long been investigated by both clinicians and engineers. One of the main issues discussed by these experts is the relationship between the contractions and the electrical activity of the stomach. It has been hypothesised that small amplitude signals with high frequency content, namely spike activity, might be responsible for triggering the contractions (YOU and CHEY, 1984). These signals are superimposed on the slow-wave depolarisations that are assumed to be generated by the dense neural network, ICC, lying among the two muscle layers, namely the longitudinal and circular muscles of the organs of the GI tract.

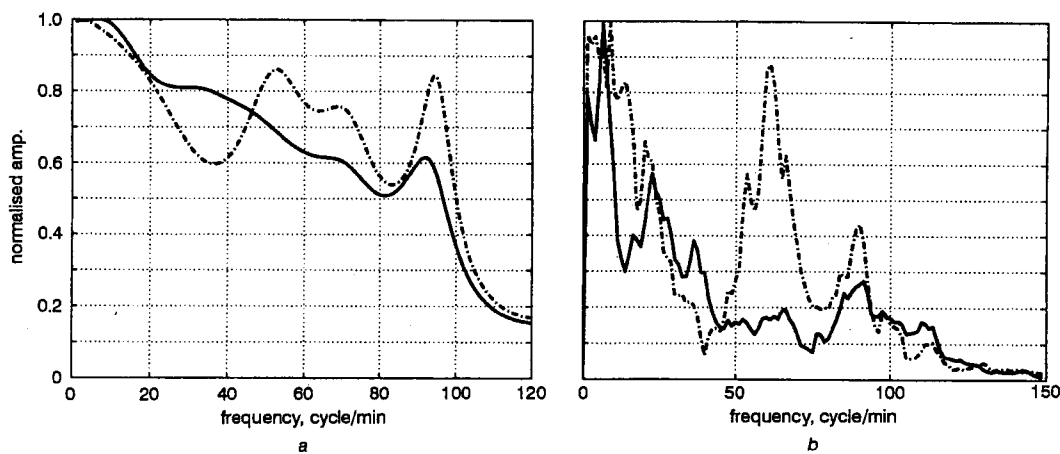


Fig. 6 PSEs from (a) AR method, and (b) BiS-based method. — no contraction, unspiked data; - - - contraction, data with spike activity. Data are obtained from Lynn Institute for Healthcare and Research

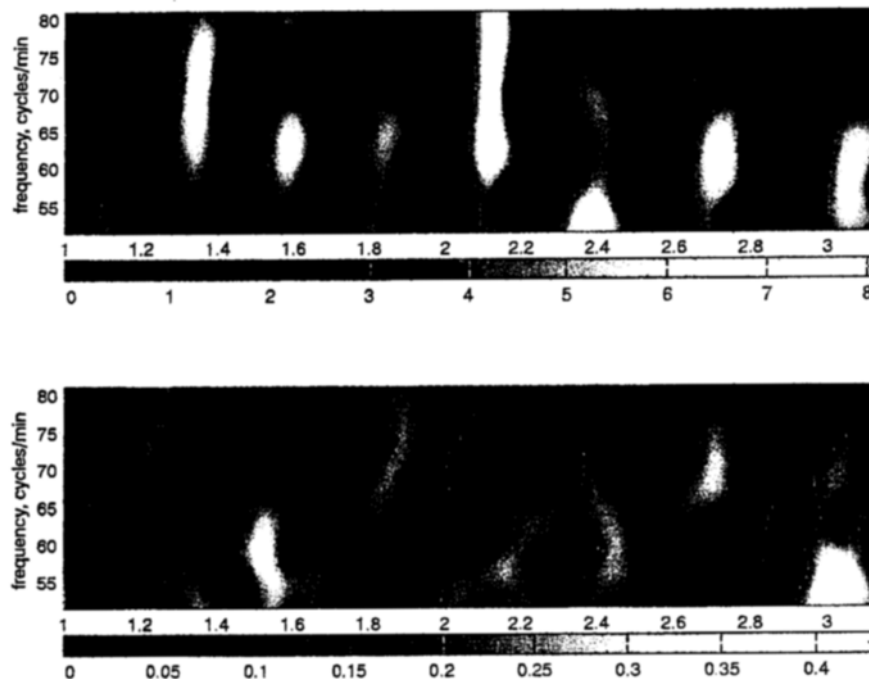


Fig. 7 CWT of serosal data (a), and surface data (b). x axis for both images is the time in minutes. Below each image, the colourbar representing the energy levels is displayed

Our aim in this paper is to detect the spike activities non-invasively from surface EGG recordings. In our studies we first identify that spike waves within a certain frequency range can penetrate the layers of the abdomen by using the correlation method and then apply the CWT method to analyse the results. Researchers have designed various experimental setups for properly detecting the rhythmic activity of the organs of the GI tract, especially the stomach and intestines. They preferred to adjust the cutoff frequency of the lowpass filter to 0.18–0.33 cycles per minute, whereas we use a higher cutoff range of 35 Hz at a sampling rate of 100 Hz to start the acquisition and then decimate the digitised signals to 4 Hz. The decimation process is incorporated because the spike activity signals are observed to cover a frequency interval from 50 to 80 cycles per minute (0.83 to 1.33 Hz). Hence a decimation to 4 Hz is preferred. The same sampling frequency is also recommended by the theoretical work of REDDY *et al.*, 1987).

We first analyse the serosal signals recorded from the stomach and evaluate the frequency range of the spike activity by using two power spectrum estimators; autoregressive and bispectrum based methods. These methods yield a range of 50–80 cycles per minute for the frequency range of the spike activity from our dog experiments. In these analyses we observe that the bispectrum-based method presents a clearer difference between spiky and unspiked data. We therefore conclude that the Gaussian nature inherent in serosal signals blurs the frequency content; thus, the bispectrum-based PSE is a better method for tracking changes in the serosal signal.

We then focus on the surface recordings to see whether there exists a correlation between serosal and surface recordings at this frequency range. We modified the method of power dynamics into an algorithm that could provide a selection of frequency ranges of interest: selective power dynamics (SPD). This method answers the questions concerning signal penetration through tissue. We then observed that the energy progression in surface signals follows that from serosal recordings. However, in certain cases the correlation between the two was not as high as expected. There are many reasons for having low correlation coefficients between serosal and surface data:

1. Serosal electrodes measure the electrical activity of a very localised site. This site usually represents the dipole ring of serosal activity; the EGG signal is an integrated activity of the whole stomach (MIRIZZI and STELLA, 1985; MIRIZZI *et al.*, 1986; FAMILONI, 1994; MINTCHEV and BOWES, 1994).
2. Spikes occur locally on the serosa of the stomach. If at any time a spike occurs at a different site from the measuring one, then the serosal electrode will not pick it up, while the surface electrode might.
3. It is not clear how the tissue layers affect the serosal signal. Smearing or filtering of the signals might lead to low correlation coefficients.
4. Interference of respiratory, EKG, motion signals and other artefacts can decrease the correlation coefficient.
5. Delay factor plays an important role. This delay may not be as a result of penetration, but rather from the horizontal distance between two recording sites. If we trace the vertical projection of the surface electrodes onto the stomach, we see that they cover a larger area (Fig. 1b). According to the quasistationary electric field formulation (PLONSEY, 1969), electrical activity generated at one point of the body is distributed to all points of the body. So spike activity occurring at a site other than the serosal recording site could also show up in the surface recording, delayed by several seconds. This delay might be responsible for low correlation as well. We tested this hypothesis by increasing the length of the analysis window, and observed that the correlation coefficient was raised to 0.92.

After observing that spike activity passes through tissue, we apply the continuous wavelet transform representing the time–frequency distribution of both recordings. The reason for choosing CWT over other representations is its high time and frequency localisation properties. We compare our results with the spectrogram and running spectrum, and conclude that the CWT yields higher clarity in enhancing high frequency signal components (QIAO, 1997). One problem with the CWT method is its computational complexity.

We are now able to detect the spike activity of the stomach from surface EGG recordings with the help of SPD and CWT methods. Nevertheless, the real problem lies not in selecting

the right algorithm, but in data acquisition. We observed during our experiments that as the surface electrodes were rotated such that their bipolar axis became perpendicular to the longitudinal axis of the stomach, correlation decreased. This is further confirmation of Mirizzi's work (MIRIZZI and STELLA, 1985; MIRIZZI *et al.*, 1986). We believe that further work is needed in improving data acquisition and electrode placement. We also suggest that a standardised EGG electrode placement should be developed as this is an important factor in EGG measurements.

Acknowledgments—The authors wish to express their thanks to Sandhill Scientific Inc, Highlands Ranch, CO for their generous support and also to Dr Tayfun Akgül and Dr Banu Onaral of Drexel University, Philadelphia, PA for their valuable input and guidance. We extend our gratitudes to Dr J. Z. Chen and his associates from the Lynn Institute for Healthcare Research, Oklahoma City, OK for allowing us to analyse their data. We also thank Dr W. Y. Chey and Dr K. Y. Lee for performing the dog experiments at the Animal Care Center, University of Rochester, NY.

References

- AKIN, A. (1998): Non-invasive detection of spike activity of the stomach from cutaneous EGG, PhD thesis, Drexel University, Philadelphia.
- AKIN, A., AKGÜL, T., CHEY, W. Y. and LEE, K. Y. (1997): 'Comparison of methods to analyze the antropyloric electrical activity', *Proc. 19th IEEE EMBS Conf.*, pp. 1602–1605.
- AKIN, A., SUN, H. H., CHEY, W. Y. and LEE, K. Y. (1998): 'Detection of spike activity from abdominal surface', *6th IEGG Workshop*, p. 15.
- ALSHEBEILI, S. A. and ÇETIN, A. E. (1990): 'A phase reconstruction algorithm from bispectrum', *IEEE Trans. Geosci., Rem. Sensing*, **28**(2), pp. 166–170.
- AMY, T. P. (1975): 'Disorders of motility', in P. B. BEESON and W. MCDERMOTT (Eds): 'Textbook of medicine' (W. B. Saunders, PA) p. 1178.
- ATANASSOVA, E., DASKALOV, I., DOTSINSKY, I. and CHRISTOV, I. (1995): 'Non-invasive electrogastrography part 1: Correlation between the gastric electrical activity in dogs with implanted and cutaneous electrodes', *Arch. Physiol., Biochem.*, **103**(4), pp. 431–435.
- BERNE, R. M. and LEVY, M. N. (1993): 'Physiology', 3rd Edn (Mosby Year-book, MO).
- BRADSHAW, L. A. (1995): Measurement and modeling of gastrointestinal bioelectric and biomagnetic fields, PhD thesis, Vanderbilt University.
- CHEN, J. D. and MCCALLUM, R. (1991): 'Electrogastrography: measurement, analysis and prospective applications', *Med. Biol. Eng. Comput.*, **29**, pp. 339–350.
- CHEN, J. D. and MCCALLUM, R. (1993): 'Clinical applications of electrogastrography', *Am. J. Gastroenterol.*, **88**(9), pp. 1324–1336.
- DUTILLEUX, P. (1987): 'An implementation of the "algorithme à trous" to compute the wavelet transform', in J. M. COMBES and A. GROSSMANN (Eds): 'Wavelets time-frequency methods and phase space', 2nd Edn (Springer Verlag).
- FAMILONI, B. O. (1994): Mathematical modeling and simulation of electrogastrograms', in J. Z. CHEN and R. W. MCCALLUM (Eds): 'Electrogastrography: principles and applications' (Raven, New York) pp. 171–196.
- GROSSMANN, A., KRONLAND-MARTINET, R. and MORLET, J. (1987): 'Reading and understanding continuous wavelet transform', in J. M. COMBES and A. GROSSMANN (Eds): 'Wavelets time-frequency methods and phase space', 2nd edn (Springer Verlag).
- KOCH, K. L. and STERN, R. M. (1994): 'Electrogastrographic data acquisition and analysis: The penn state experience', in CHEN, J. Z. and MCCALLUM, R. W. (Eds): 'Electrogastrography: principles and applications' (Raven, New York) pp. 31–44.
- LIU, L. W. C., SPERELAKIS, N. and HUIZINGA, J. D. (1995): 'Pacemaker activity and intercellular communication in the gastrointestinal musculature', in J. D. HUIZINGA (Ed.): 'Pacemaker activity and intercellular communication' (CRC Press, Boca Raton).
- MINTCHEV, M. and BOWES, K. (1997): 'Computer model of gastric electrical stimulation', *Ann. Biomed. Eng.*, **25**, pp. 726–730.
- MINTCHEV, M. P., STICKEL, A. and BOWES, K. L. (1997a): 'Comparative assessment of power dynamics of gastric electrical activity', *Dig. Dis. Sci.*, **42**(6), pp. 1154–7.
- MINTCHEV, M. P., STICKEL, A., OTTO, S. J. and BOWES, K. L. (1997b): 'Reliability of percent distribution of power of the electrogastrogram in recognizing gastric electric uncoupling', *IEEE Trans. Biomed. Eng.*, **44**(12), pp. 1288–1291.
- MINTCHEV, M. P. and BOWES, K. L. (1994): 'Capabilities and limitations of electrogastrograms', in CHEN, J. Z. and MCCALLUM, R. W. (Eds.): 'Electrogastrography: principles and applications' (Raven, New York) pp. 154–169.
- MIRIZZI, N., STELLA, R. and SCAFOGLIERI, U. (1985): 'A model of extracellular waveshape of the gastric electrical activity', *Med. Biol. Eng. Comput.*, **23**, pp. 33–37.
- MIRIZZI, N., STELLA, R. and SCAFOGLIERI, U. (1986): 'Model to simulate the gastric electrical control and response activity on the stomach wall and on the abdominal surface', *Med. Biol. Eng. Comput.*, **24**, pp. 157–163.
- MORLET, J. G., ARENS, G. and FOURGESU, I. (1982): 'Wave propagation and sampling theory', *Geophysics*, **47**, pp. 203–236.
- NIKIAS, L. C. and PETROPULU, A. P. (1993): 'Higher-order spectra analysis: a nonlinear signal processing framework' (Prentice Hall, New Jersey).
- PLONSEY, R. W. (1969): 'Bioelectric phenomena' (McGraw-Hill, New York).
- PROAKIS, J. G. and MANOLAKIS, D. G. (1996): 'Digital signal processing, principles, algorithms, and applications' (Prentice Hall, New Jersey).
- QIAO, W. (1997): Continuous wavelet analysis as an aid in the representation and interpretation of electrogastrographic signals, PhD thesis, Drexel University, Philadelphia.
- REDDY, S. N., COLLINS, S. M. and DANIEL, E. E. (1987): 'Frequency analysis of gut emg', *Crit. Rev. Biomed. Eng.*, **15**(2), pp. 95–116.
- RIOUL, O. and DUHAMEL, P. (1992): 'Fast algorithms for discrete and continuous wavelet transform', *IEEE Trans. Inform. Theory*, **38**(2), pp. 569–586.
- SANDERS, K. M. (1996): 'A case for interstitial cells of cajal as pacemakers and mediators of neurotransmission in the gastrointestinal tract', *Gastroenterology*, **111**, pp. 492–515.
- SMOUT, A. J. P. M., van der SCHEE, J. and GRASHUIS, L. L. (1980): 'What is measured in electrogastrography?', *Dig. Dis. Sci.*, **25**, pp. 179–187.
- STRANG, G. and NGUYEN, T. (1996): 'Wavelets and filter banks' (Wellesley-Cambridge Press, MA).
- VETTERLI, M. and HARLEY, C. (1992): 'Wavelets and filter banks: theory and design', *IEEE Trans. Sig. Process.*, **40**(9), pp. 2207–2232.
- YOU, C. Y. and CHEY, W. Y. (1984): 'Study of electromechanical activity of the stomach in humans and in dogs with particular attention to tachygastria', *Gastroenterology*, **86**, pp. 1460–8.

Authors' biographies

HUN H. SUN received his BSEE degree from Chiao Tung University, Shanghai, China, in 1946, a MSEE degree from the University of Washington, Seattle, in 1949, and his PhD degree from Cornell University, Ithaca, NY, in 1955. He joined Drexel University, Philadelphia, PA, in 1953, and served as Director of Biomedical Engineering, from 1964 to 1974, and Chairman of Electrical Engineering, from 1973 to 1978. He is now the Ernst O. Lange Professor of Electrical Engineering at Drexel University. Dr Sun has served on various committees including the AdCom of the IEEE Engineering in Medicine and Biology Society, Translation Relations Committee, Standard Committee, and on the board of Alliance of the Biomedical Engineering Societies. He has served as Editor-in-chief of *IEEE Transactions on Biomedical Engineering*, and Editor-in-chief of the *Annals of Biomedical Engineering* and been on the Editorial Board of *Automedica*. He has been a member of the Study Committee on Surgery

and Bioengineering in NIH, and member of Visiting Committee in Critical and Engineering Technologies Division in NSF.

ATA AKIN received a BS degree in Electronics and Telecommunications Engineering in 1993, and MS in Biomedical Engineering in

1995, both from Istanbul Technical University, Istanbul, Turkey; and a PhD from the School of Biomedical Engineering, Science and Health Systems, Drexel University, Philadelphia in 1998. His current research interests are biomedical signal processing, medical instrumentation and bio-optics.